N_H-N_HI correlation in gigahertz-peaked-spectrum galaxies

(Article begins on next page)

19 April 2024

N_{H} - N_{HI} correlation in gigahertz-peaked-spectrum galaxies [⋆]

L. Ostorero[1,2,⋆⋆], **R. Morganti**[3,4], **A. Diaferio**[1,2], **A. Siemiginowska**[5], **Ł. Stawarz**[6], **R. Moderski**[7], and **A. Labiano**[8]

[1] Dipartimento di Fisica, Università degli Studi di Torino, Via P. Giuria 1, 10125 Torino, Italy
[2] Istituto Nazionale di Fisica Nucleare (INFN), Via P. Giuria 1, 10125 Torino, Italy
[3] Netherlands Institute for Radio Astronomy, Postbus 2, 7990 AA Dwingeloo, The Netherlands
[4] Kapteyn Astronomical Institute, University of Groningen, P.O. Box 800, 9700 AV Groningen, The Netherlands
[5] Harvard-Smithsonian Center for Astrophysics, 60 Garden St., Cambridge, MA 02138, USA
[6] Astronomical Observatory, Jagiellonian University, ul. Orla 171, 30-244 Kraków, Poland
[7] Nicolaus Copernicus Astronomical Center, Bartycka 18, 00-716 Warsaw, Poland
[8] Institute for Astronomy, Department of Physics, ETH Zurich, CH-8093 Zurich, Switzerland

With the Westerbork Synthesis Radio Telescope, we performed HI observations of a sample of known X-ray emitting Gigahertz-peaked-spectrum galaxies with compact-symmetric-object morphology (GPS/CSOs) that lacked an HI absorption detection. We combined radio and X-ray data of the full sample of X-ray emitting GPS/CSOs and found a significant, positive correlation between the column densities of the total and neutral hydrogen (N_{H} and N_{HI}, respectively). Using a Bayesian approach, we simultaneously quantified the parameters of the N_{H} - N_{HI} relation and the intrinsic spread of the data set. For a specific subset of our sample, we found $N_{\mathrm{H}} \propto N_{\mathrm{HI}}{}^{b}$, with $b = 0.93^{+0.49}_{-0.33}$, and $\sigma_{\mathrm{int}}(N_{\mathrm{H}}) = 1.27^{+1.30}_{-0.40}$. The N_{H} - N_{HI} correlation suggests a connection between the physical properties of the radio and X-ray absorbing gas.

1 Introduction

Compact radio galaxies with GHz-peaked spectrum (GPS) and compact-symmetric-object (CSO) morphology, hereafter referred to as GPS/CSOs, are powerful, sub-kiloparsec scale sources that likely represent the youngest fraction of the radio galaxy population (e.g., O'Dea 1998; Orienti 2016). Their radio emission is dominated by the mini-lobes, fully contained in the host galaxy interstellar medium. Although they are increasingly detected in the X-ray domain (O'Dea et al. 2000; Risaliti et al. 2003; Guainazzi et al. 2004, 2006; Vink et al. 2006; Siemiginowska et al. 2008; Tengstrand et al. 2009), the best angular resolution currently available ($\sim 1''$ with *Chandra*) is not sufficient to resolve the X-ray morphology of most GPS/CSOs. Therefore, the origin of their X-ray emission is still matter of debate (e.g., Siemiginowska et al. 2009; Migliori 2016).

Both the radio and the X-ray emission display significant absorption. However, the location of the radio and X-ray absorbers in the host galaxy of the radio source are still debated too. In the limited sample of compact sources with available high angular resolution HI absorption measurements, the HI is typically detected against one or both radio lobes (Araya et al. 2010, and references therein; Morganti et al. 2013), with estimated covering factors, C_{f}, vari-

able from ~ 0.2 to ~ 1 (e.g., Peck et al. 1999; Morganti et al. 2004). The general consensus is that the HI absorber has an inhomogeneous or clumpy nature, although the actual distribution of the gas is not known.

Hard X-ray (2–10 keV) spectra of GPS/CSOs reveal a mean value of the column density much higher than that of a control sample of exended radio galaxies of the FR-I type (whose core emission appears to be generally unobscured by an optically thick torus), and intermediate between the values of unobscured and highly obscured FR-II radio galaxies, where the presence of an optically thick torus is supported by optical and X-ray observations (Tengstrand et al. 2009, and references therein). Any relationship between the radio and X-ray absorbers may thus help to clarify the absorption picture.

A comparison between the X-ray and HI column densities, N_{H} and N_{HI} respectively, in a sample of GPS/CSOs showed that the N_{H} values are systematically higher than the N_{HI} values of 1–2 orders of magnitudes (Vink et al. 2006; Tengstrand et al. 2009). Because the estimate of N_{HI} depends on the ratio between the spin temperature of the absorbing gas and its source covering factor, $T_{\mathrm{s}}/C_{\mathrm{f}}$ (see Equation 2), the magnitude of this offset can change according to the $T_{\mathrm{s}}/C_{\mathrm{f}}$ parameter, which is poorly constrained (Ostorero et al. 2010, and references therein; Curran et al. 2013). Regardless of its magnitude, however, the existence of a systematic offset might in itself indicate a connection between

---

Table 1 GPS/CSO sources of our sample: source names, optical redshifts, type of N_{HI} data (from spatially unresolved measurements) and of N_H data included in the present analysis (V: value, UL: upper limit, NA: not available because of bad data quality, IP: analysis in progress) and corresponding references (⋆: this work, and Ostorero et al., in prep.; ⋆⋆: Siemiginowska et al., in prep.; numbers refer to papers cited in the reference list, where they are included in square brackets).

Source name (B1950)	z_{opt}	N_{HI}	Ref.	N_H	Ref.
0026+346	0.517	NA	⋆	V	9
0108+388	0.66847	V	1	LL	10
0116+319	0.06	V	2	IP	⋆⋆
0428+205	0.219	V	3	UL	10
0500+019	0.58457	V	4	V	10
0710+439	0.518	NA	⋆	V	10
0941-080	0.228	V	⋆	UL	11,12
1031+567	0.450	V	⋆	V	10
1117+146	0.362	UL	⋆	UL	10
1323+321	0.370	V	3	V	10
1345+125	0.12174	V	5	V	10,12
1358+624	0.431	V	3	V	10
1404+286	0.07658	V	1	V	13
1607+268	0.473	UL	⋆	UL	10
1843+356	0.764	UL	⋆	IP	⋆⋆
1934-638	0.18129	V	6	UL	14
1946+708	0.101	V	7,8	V	14
2008-068	0.547	NA	⋆	UL	10
2021+614	0.227	UL	⋆	IP	⋆⋆
2128+048	0.99	UL	⋆	V,UL	9,10
2352+495	0.2379	V	3	V	10

X-ray and radio absorbers, and deserves to be investigated statistically.

In a sample of 10 GPS/CSOs, whose N_H and N_{HI} measurements were available in the literature, we discovered a significant, positive N_H-N_{HI} correlation (Ostorero et al. 2009, 2010), with N_H and N_{HI} linked through the relationhsip $N_H \propto N_{HI}{}^b$, with $b \simeq 1$. With the aim of improving the statistics of the N_H-N_{HI} correlation sample, we carried out a program of observations of the known X-ray emitting GPS/CSOs lacking an HI absorption detection with the Westerbork Synthesis Radio Telescope (WSRT). In this paper, we report the first results of this project.

2 Source sample

We studied the HI and X-ray absorption properties of the full sample of GPS galaxies known as X-ray emitters to date. This sample is composed of 21 sources, belonging to at least one of the following GPS samples: Stanghellini et al. (1998), Snellen et al. (1998), Torniainen et al. (2007), and Vermeulen et al. (2003). All of these sources were also classified as CSOs. The source list is given in Table 1.

3 HI observations with the WSRT

With the WSRT, we searched for HI absorption the 10 sources of our sample (marked with a star in Column 4 of Table 1) that still lacked an HI detection, either because they were never observed or because previous observations yielded only upper limits to the HI optical depth.

Each target was observed for an exposure time of four to 12 hours with the UHF-high-band receiver (appropriate when $z \gtrsim 0.2$) in dual orthogonal polarisation mode. The observing band was 10 to 20 MHz wide, with 1024 spectral channels, and was centered at the frequency where the HI absorption line is expected to occur based on the optical redshift. Compared to the HI survey of compact sources by Vermeulen et al. (2003), our observations could benefit from a larger ratio between number of spectral channels and observing band width: this improvement, together with the longer exposure times, enabled a more effective separation of narrow HI absorption features from radio frequency interferences (RFI) in most of the previously observed sources. The data reduction process and the results of the analysis will be presented elsewhere.

We detected HI absorption in two out of 10 targets. For five targets, we could estimate upper limits to the line optical depth and to the HI column density. For three of our targets, RFI were too strong to obtain any useful data (see Table 1).

The atomic hydrogen column density (in cm^{-2}) along the line of sight is related to the velocity integrated optical depth of the 21-cm absorption via the following relationship (Wolfe & Burbidge 1975):

$$N_{HI} = 1.823 \times 10^{18} T_s \int \tau \, dv. \tag{1}$$

In the optically thin regime (i.e. for $\tau \lesssim 0.3$), Equation 1 is approximated by

$$N_{HI} \approx 1.823 \times 10^{18} (T_s/C_f) \int \tau_{obs} \, dv, \tag{2}$$

where $\tau_{obs} \equiv \Delta S/S$ is the observed optical depth of the line, given by the ratio between the spectral line depth (ΔS) and the continuum flux (S) of the background radio source, and is related to the actual optical depth through $\tau \approx \tau_{obs}/C_f$. For homogeneity with literature data, we estimated the HI column densities by assuming that the absorber fully covers the radio source (C_f=1) and that the spin temperature is T_s=100 K. These assumptions yielded N_{HI} values that are lower limits to the actual column densities. When no HI line was detected, upper limits to N_{HI} were estimated from the optical depth upper limits ($\tau_{3\sigma}$) that we derived from the 3-σ noise level.

4 N_H - N_{HI} correlation

We investigated the existence of a correlation between the neutral hydrogen column density (N_{HI}) and the total hydrogen column density (N_H), with the aim of either confirming or disproving the significant, positive N_H-N_{HI} correlation

that we discovered for a smaller sample of 10 GPS/CSOs (Ostorero et al. 2009, 2010). Below, we describe the selection of the correlation sample and present the first results of the correlation analysis.

4.1 N_{HI} **sample**

HI absorption detections and corresponding N_{HI} values were available for 13 out of 21 sources of the sample; N_{HI} upper limits could be estimated for five sources; for three sources, no useful data were obtained (see Table 1).

Because multiple spectral features were detected in the HI absorption spectra of a subsample of sources, different N_{HI} values could be associated to the same source. Here, we present the result of the analysis that we performed by taking the *total* N_{HI} of the detected absorption features into account. The full record of cases will be presented elsewhere. When more than one total N_{HI} estimate was available for a given source, we chose the most recent result from spatially unresolved measurements.

4.2 N_H **sample**

Estimates of the total hydrogen column densities (N_H) were available for 18 out of 21 sources: 11 of them are N_H values, six of them are upper limits, and one of them is a lower limit to N_H. For the remaining sources, the analysis is in progress (see Table 1).

The N_H estimates were derived from the X-ray spectral analysis by fitting a model spectrum, absorbed by both a Galactic and a local (i.e., at redshift z_{opt}) gas column density, to the observed X-ray spectrum; in the fitting procedure, the N_H parameter was left free to vary. For some sources, more than one model could be fit to the spectrum, yielding different N_H best-fit estimates. In particular, four sources (1404+286, 1607+268, 1934-638, and 1946+708) could satisfactorily be interpreted as both Compton-thin and Compton-thick X-ray sources: here, we present the analysis performed by taking the Compton-thin N_H values only into account; the full record of cases will be discussed elsewhere. Furthermore, for one source (0108+388), the available lower limit to N_H is consistent with both a Compton-thin and a Compton-thick scenario: again, here we present the results of the analysis performed under the assumption that the source is Compton-thin. For five sources of the sample, different N_H estimates were derived from observations carried out in different epochs. Because we cannot rule out long-term column-density variations, when different values were not consistent with each other at the 1σ level (as for 1345+125) and when both values and upper limits were available (as for 2128+048), we chose to include the two extreme N_H estimates in our correlation sample, each of them associated to the same N_{HI} value. Including either the average or any of the two N_H estimates does not change our results significantly.

4.3 N_H - N_{HI} **sample**

Pairs of N_{HI} and N_H *values* (V-V pairs in Table 1) were available for a subsample of eight sources, hereafter referred to as the *detection correlation sample*, D. We also define a second *detection correlation sample*, D', which includes, besides the sources of sample D, source 0108+388, for which a proper detection is not available. Under the assumption that the source is Compton thin (see Sect. 4.2) an N_H value can be estimated as the mean of the 3-σ lower limit and the physical upper bound of the Compton-thin N_H range (i.e., $N_H = 9.0 \times 10^{23}$ cm^{-2}). We consider the N_H range as a $\pm 3\sigma$ interval, and thus associate to the mean N_H the corresponding 1σ error. Pairs of N_{HI} and N_H *estimates* (i.e., pairs including detections and/or upper limits: V-V, V-UL, UL-V, and UL-UL pairs in Table 1) were available for a subsample of 14 sources, hereafter referred to as the *estimate correlation sample*, E. As we did for the detections, we also define a second *estimate correlation sample*, E', which includes sample E and source 0108+388.

4.4 **Correlation analysis**

Figures 1 and 2 display the (N_{HI},N_H) data for the *detection* and *estimate correlation samples*, respectively.

First, we performed the correlation analysis on the *detection correlation sample*. A Pearson correlation analysis applied to sample D did not reveal a significant correlation. This result is confirmed by the more robust, *non-parametric* (or *rank*) methods, i.e. Spearman's and Kendall's correlation analysis (Press 1992). The main reason why we do not confirm the result found for the detections in our previous paper (Ostorero et al. 2009, 2010) is that we replaced the N_H values that were derived by fixing the X-ray spectral index (Vink et al. 2006) with more robust estimates (Tengstrand et al. 2009). We also chose to include source 1404+286 (with a complex X-ray spectrum) in our sample.

We then repeated the Pearson correlation analysis for sample D', and we find a positive, significant correlation (correlation coefficient: $r = 0.93$; probability of the null-hypothesis of no correlation being true: $P = 7.8 \times 10^{-5}$). The statistical significance of this correlation, however, is admittedly driven by source 0108+388, characterized by the largest (N_{HI},N_H) values. Indeed, in the same sample, the evaluation of the correlation by means of the more robust Spearman's and Kendall's correlation analysis dramatically decreased the significance of the above result ($P = 0.3$).

In the *estimate correlation sample*, we investigated the correlation by means of survival analysis techniques. In particular, we made use of the software package ASURV Rev. 1.3[1] (Lavalley, Isobe & Feigelson 1992), which implements the methods for bivariate problems presented in Isobe, Feigelson & Nelson (1986). The ASURV generalized Spearman's and Kendall's correlation analysis applied to sample E shows that the data are significantly correlated ($P = 1.8 \times 10^{-2} -$
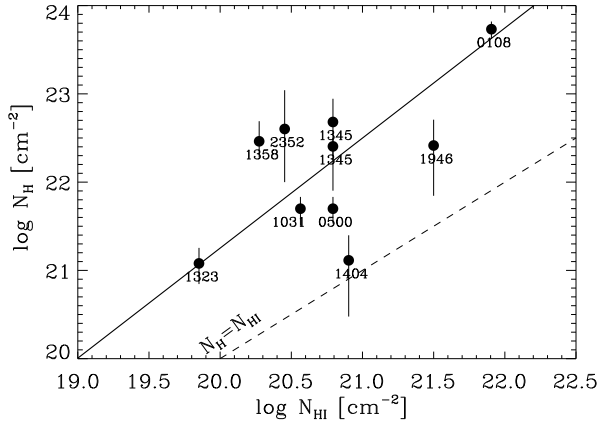
---

[1] http://www2.astro.psu.edu/statcodes/asurv/

Fig. 1 X-ray column densities ($N_{\rm H}$) as a function of radio column densities ($N_{\rm HI}$) for the D'_1 sample. The solid symbols show the ($N_{\rm HI}$,$N_{\rm H}$) measurements with 1σ error bars on $N_{\rm H}$. $N_{\rm HI}$ was computed by assuming $T_{\rm s} = 100$ K and $C_{\rm f} = 1$. Labels show a shortened version of the source names reported in Table 1. Solid line: linear regression best-fit line to the data (to guide the eye; $\log N_{\rm H} = a + b \log N_{\rm HI}$, with $a = -3.68$ and $b = 1.25$); dashed line: bisector of the $N_{\rm HI}$-$N_{\rm H}$ plane. Data are from references listed in Table 1.

Fig. 2 X-ray column densities ($N_{\rm H}$) as a function of radio column densities ($N_{\rm HI}$) for the E'_1 sample. The solid symbols show the ($N_{\rm HI}$,$N_{\rm H}$) measurements with 1σ error bars on $N_{\rm H}$. $N_{\rm HI}$ was computed by assuming $T_{\rm s} = 100$ K and $C_{\rm f} = 1$. Arrows represents upper limits. Labels show a shortened version of the source names reported in Table 1. Solid line: linear regression best-fit line to the data (to guide the eye; $\log N_{\rm H} = a + b \log N_{\rm HI}$, with $a = -9.8$ and $b = 0.59$); dashed line: bisector of the $N_{\rm HI}$-$N_{\rm H}$ plane. Data are from references listed in Table 1.

3.8×10^{-2}). For sample E', including source $0108+388$[2] the significance improved further ($P = 6.5 \times 10^{-3} - 9 \times 10^{-2}$).

As far as the law describing the relationship between $N_{\rm H}$ and $N_{\rm HI}$ is concerned, according to Pearson's test we could fit a linear relation to the *detection sample* D': $\log N_{\rm H} = a + b \log N_{\rm HI}$, with $a = -3.68 \pm 1.72$ and $b = 1.25 \pm 0.08$. However, this relation is not a good description of the data ($\chi^2_{\rm red} = 6.73$): the dispersion of the data is clearly larger than the typical uncertainties on $N_{\rm H}$ (see Fig. 1).

As for the *estimate samples*, E and E', the ASURV Schmitt's linear regression enabled us to perform a linear fit to the data (the estimated best-fit slope is $b = 0.59$) but not to evaluate the goodness of the fit. A visual inspection of this data set again confirms a dispersion larger than the typical $N_{\rm H}$ uncertainties (see Fig. 2). This fact suggests that additional variables are involved in the correlation, and the $N_{\rm H}$ - $N_{\rm HI}$ relation is the two-dimensional projection of a more complex relation.

4.5 Bayesian analysis

In order to derive the correlation parameters of the $N_{\rm H}$ - $N_{\rm HI}$ relation and the intrinsic scatter of the data set, it is appropriate to resort to Bayesian analysis. Given our data set $DS = \{x^i, y^i, S_1^i, S_2^i\}$, where $\{x^i\} = \{\log N_{\rm HI}\}$ and $\{y^i\} = \{\log N_{\rm H}^i\}$ are the vectors of the $\log N_{\rm HI}$ and $\log N_{\rm H}$ values, respectively, $\{S_1^i\}$ and $\{S_2^i\}$ are the vectors of the upper and lower uncertainties on the $\{y^i\}$ values, and i runs

Fig. 3 Bayesian analysis applied to sample D'_1. The solid symbols show the ($N_{\rm HI}$,$N_{\rm H}$) measurements with 1σ error bars on $N_{\rm H}$. The solid, straight-line is the $N_{\rm H}$ - $N_{\rm HI}$ relation: $\log N_{\rm H} = a + b \log N_{\rm HI}$, with $a = 2.78$ and $b = 0.93$. The dotted lines show the $\pm \sigma_{\rm int}$ standard deviation of the relation, with $\sigma_{\rm int} = 1.27$. $N_{\rm HI}$ was computed by assuming $T_{\rm s} = 100$ K and $C_{\rm f} = 1$.

from 1 to the number of data points, N, we determined the multi-dimensional probability density function (PDF) of the parameters $\theta = \{a, b, \sigma_{\rm int}\}$. Here, a and b are the parameters of the correlation: $y = a + bx$. In order to mimic additional hidden parameters in the relation, we assumed that y^i is a random variate with mean $\bar{y}^i = a + bx^i$ and variance $\sigma_{\rm int}^2$, with $\sigma_{\rm int}$ the intrinsic scatter of the dependent variable (e.g., Andreon & Hurn 2010).

---

[2] for $0108+388$, we still use the $N_{\rm H}$ value estimated as described in Sect. 4.2, instead of the lower limit, because ASURV cannot deal with two types of data censoring.
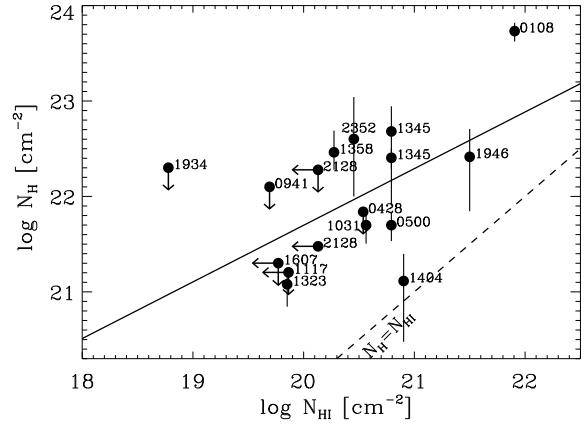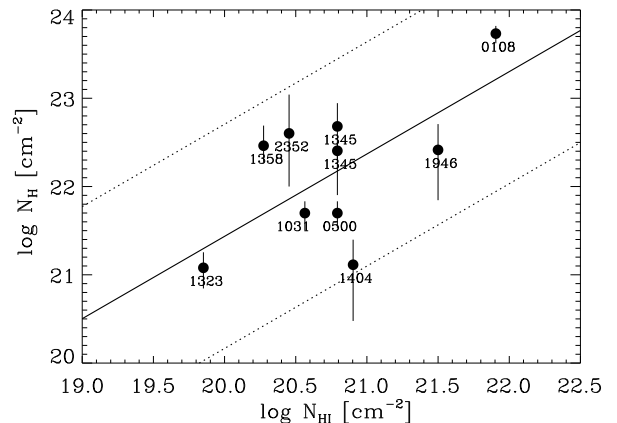
For our Bayesian analysis, we used the code APEMoST[3], developed by J. Buchner and M. Gruberbauer (e.g., Gruberbauer 2009). Because this code cannot deal with censored data, we restrict our Bayesian analysis to the *detection sample D'*. We assumed independent flat priors for parameters a and b, except for the internal dispersion σ_{int}, which is positive defined. We use 2×10^6 MCMC iterations to guarantee a fairly complete sampling of the parameter space. The boundaries of the parameter space were set to $[-1000, 1000]$ for the a and b parameters, $[0.01, 1000]$ for the σ_{int} parameters. The initial seed of the random number generator was set with the `bash` command `GSL_RANDOM_SEED=$RANDOM`.

Our analysis shows that, for any given value of $\log N_{HI}$, $\log N_H$ takes the value $\log N_H = a + b \log N_{HI} \pm \sigma_{int}$ (with $a = 2.78^{+6.82}_{-9.83}$, $b = 0.93^{+0.49}_{-0.33}$, and $\sigma_{int} = 1.27^{+1.30}_{-0.40}$) with a 68 percent probability. As an example, when N_{HI} is equal to 10^{20} cm^{-2}, N_H varies in the interval $(10^{20.11} - 10^{22.65})$ cm^{-2}. Although both σ_{int} and the uncertainties on a, b, and σ_{int} are large, the N_H - N_{HI} relation derived from the Bayesian analysis properly describes our data set, unlike the linear relations derived in Sect. 4.4. The results of the Bayesian analysis are displayed in Fig. 3.

5 Conclusions

We performed spatially unresolved HI absorption observation of a sample of GPS/CSO galaxies with the WSRT, with the aim of improving the statistics of the N_H -N_{HI} correlation sample. We confirmed a significant, positive correlation between N_H and N_{HI}. For the full, censored data set, the generalized linear regression analysis yields $N_H \propto N_{HI}{}^b$, with $b \simeq 0.6$, although the goodness of this fit cannot be evaluated. For the detection subset, the linear regression analysis yields $N_H \propto N_{HI}{}^b$, with $b \simeq 1$, however the χ^2 is large. This fact may indicate that the N_H - N_{HI} relation is not a one-to-one relation: additional variables are involved in the correlation and generate the intrinsic spread of the data set. The Bayesian analysis applied to the detection subset enabled us to simultaneously quantify (i) the parameters of the N_H - N_{HI} relation whose slope is $b = 0.93^{+0.49}_{-0.33}$, and (ii) the intrinsic spread on N_H, $\sigma_{int} = 1.27^{+1.30}_{-0.40}$. The N_H - N_{HI} correlation suggests a connection between the intrinsic properties of the X-ray and HI absorbers. We are currently investigating the implications of this correlation, and we are attempting to identify and constrain the additional variables responsible for the intrinsic spread.

References

Andreon, S., Hurn, M.A.: 2010, MNRAS 404, 1922

Araya, E.D., Rodríguez, C., Pihlström, Y., Taylor, G.B., Tremblay, S., Vermeulen, R.C.: 2010, AJ 139, 17

Carilli, C.L., Menten, K.M., Reid, M.J., Rupen, M.P., Yun, M.S.: 1998, ApJ 494, 175 [4]

Curran, S.J., Allison, J.R., Glowacki, M., Whiting, M.T., Sadler, E.M. : 2013, MNRAS 431, 3408

Guainazzi, M., Siemiginowska, A., Rodriguez-Pascual, P., Stanghellini, C.: 2004, A&A 421, 461 [13]

Guainazzi, M., Siemiginowska, A., Stanghellini, C., Grandi, P., Piconcelli, E., Azubike Ugwoke, C.: 2006, A&A 446, 87 [9]

Gruberbauer, M., Kallinger, T., Weiss, W.W., Guenther, D.B.: 2009, A&A 506, 1043

Gupta, N., Salter, C.J., Saikia, D.J., Ghosh, T., Jeyakumar, S.: 2006, MNRAS 373, 972 [2]

Isobe, T., Feigelson, E.D., Nelson, P.I.: 1986, ApJ 306, 490

La Valley, M.P., Isobe, T., Feigelson, E.D.: 1992, BAAS 24, 839

Migliori, G.: 2016, this Volume

Mirabel, I.F., Sanders, D.B., Kazès, I.: 1989, ApJ 340, L9 [5]

Morganti, R., Oosterloo, T.A., Tadhunter, C.N., Vermeulen, R., Pihlström, Y.M., van Moorsel, G., Wills, K.A.: 2004, A&A 424, 119

Morganti, R., Fogasy, J., Paragi, Z., Oosterloo, T., Orienti, M.: 2013, Science 341, 1082

Orienti, M.: 2016, this Volume

Orienti, M., Morganti, R., Dallacasa, D.: 2006, A&A 457, 531 [1]

O'Dea, C.P.: 1998, PASP 110, 493

O'Dea, C.P., de Vries, W.H., Worrall, D.M., Baum, S., & Koekemoer, A.: 2000, AJ 119, 478

Ostorero, L., Moderski, R., Stawarz, Ł., Begelman, M.C., Diaferio, A., Kowalska, I., Kataoka, J., Wagner, S.J.: 2009, AN 330, 275

Ostorero, L., Moderski, R., Stawarz, et al.: 2010, ApJ 715, 1071 [11]

Peck, A.B., Taylor, G.B. Conway, J.E.: 1999, ApJ 521, 103 [8]

Pihlström, Y.M., Conway, J.E., Vermeulen, R.C.: 2003, A&A 404, 871 [7]

Press, W.H., Teukolsky, S.A., Vetterling, W.T., Flannery, B.P.: 1992, Numerical recipes in FORTRAN. The art of scientific computing (2nd ed.; Cambridge: Cambridge Univ. Press)

Risaliti, G., Woltjer, L., Salvati, M.: 2003, A&A 401, 895 [14]

---

[3] Automated Parameter Estimation and Model Selection Toolkit; http://apemost.sourceforge.net/, Feb. 2011.

Siemiginowska, A., La Massa, S., Aldcroft, T., Bechtold, J., Elvis, M.: 2008, ApJ 684, 811 [12]

Siemiginowska, A.: 2009, AN 330, 264

Snellen, I.A.G., Schilizzi, R.T., de Bruyn, A.G., Miley, G.K., Rengelink, R.B., Roettgering, H.J., Bremer, M.N.: 1998, A&AS 131, 435

Stanghellini, C., O'Dea, C.P., Dallacasa, D., Baum, S.A., Fanti, R., Fanti, C.: 1998, A&AS 131, 303

Tengstrand, O., Guainazzi, M., Siemiginowska, A., Fonseca Bonilla, N., Labiano, A., Worrall, D.M., Grandi, P., Piconcelli, E.: 2009, A&A 501, 89 [10]

Torniainen, I., Tornikoski, M., Lähteenmäki, A., Aller, M.F., Aller, H.D., Mingaliev, M.G.: 2007, A&A 469, 451

Vermeulen, R.C., Pihlström, Y. M., Tschager, W., et al.: 2003, A&A 404, 861 [3]

Véron-Cetty, M.-P., Woltjer, L., Staveley-Smith, L., Ekers, R.D.: 2000, A&A 362, 426 [6]

Vink, J., Snellen, I., Mack, K.-H., Schilizzi, R.: 2006, MNRAS 367, 928

Wolfe, A.M. Burbidge, G.R.: 1975, ApJ 200, 548